ELSEVIER

Contents lists available at ScienceDirect

International Journal of Pharmaceutics: X

journal homepage: www.sciencedirect.com/journal/international-journal-of-pharmaceutics-x



Developing Immunoniosomes (INs): Antibody and Fab conjugations of niosomal nanoparticles via UV-NBS and EDC/NHS chemistry for treating glioblastoma cells

Nilufer Cakir ^{a,b,c}, Hatice Oncel ^b, Aylin Ozkan ^b, Dilan Bicak ^b, Sibel Akgun Bas ^b, Nur Mustafaoglu ^{a,c,*}

ARTICLE INFO

Keywords: Antibody-conjugated nanoparticles Bevacizumab Glioblastoma multiforme Niosome Site-specific conjugation UV-NBS EDC/NHS Drug delivery

ABSTRACT

Antibody-conjugated nanoparticles (ACNPs), particularly immunoliposomes (ILs), have gained significant attention in cancer treatment due to their enhanced efficacy and superior tissue penetration. However, their high production costs and technical challenges underscore the need for more cost-effective alternatives. Niosomes, with their lower production costs, improved stability, and biocompatibility, have emerged as promising alternatives to liposomes in drug delivery. This study introduces immunoniosomes (INs), a novel class of antibodyconjugated niosomes, through two conjugation strategies: (i) UV-NBS, a site-specific covalent conjugation method utilizing an indole ring structure for moderate binding to the variable regions of antibodies and Fab fragments, and (ii) EDC/NHS chemistry, which conjugates antibodies to carboxylated niosomes via primary amines on lysine sidechains. Bevacizumab, a monoclonal antibody targeting VEGF and approved for the treatment of various cancers including glioblastoma multiforme (GBM), was used as a model therapeutic. Both Bevacizumab and its Fab fragment were conjugated to niosomes and evaluated in U87 glioma cells (overexpressing VEGF) and human umbilical vein endothelial cells (HUVECs) (representing normal VEGF expression). Physicochemical characterization of the conjugated niosomes confirmed hydrodynamic sizes ranging from 100 to 200 nm, neutral surface charge, and dispersity indices below 0.5-properties critical for effective cellular penetration and drug delivery. Cellular toxicity assays, conducted at a $10 \times$ dilution from commonly reported concentrations, highlighted the role of the autocrine loop in U87 glioblastoma cells, Importantly, specific Nio-Fab conjugate formulations, created through both site-specific and randomized conjugation strategies, exhibited enhanced cytotoxicity toward U87 cells while sparing healthy endothelial HUVEC cells. In summary, this research establishes novel conjugation strategies to produce stable, site-specific, and randomized antibodyniosomal conjugates with enhanced half-life and selective toxicity against GBM cells. By offering an alternative route for antibody delivery through niosomal nanocarriers, these findings open new avenues for the development of more effective GBM therapeutics, warranting further non-clinical and clinical investigations.

1. Introduction

The use of antibody-conjugated nanoparticles (ACNPs) for drug delivery has emerged a prominent area of research, primarily due to their enhanced efficacy and superior tissue penetration in cancer treatment (Arruebo et al., 2009; Kirpotin et al., 2012; Kumari et al., 2023). Among these, liposome-based ACNPs, commonly referred as immunoliposomes (ILs), have garnered significant attention for their potential in cancer

immunotherapy (Eloy et al., 2017; Kontermann, 2006; Merino et al., 2018; Rabenhold et al., 2015; Rodallec et al., 2018; Wang et al., 2018). Recent advancements in molecular engineering have facilitated the development of multivalent and multi-specific ILs, enabling complex biological interactions and improved therapeutic outcomes (Rabenhold et al., 2015; Rodallec et al., 2018). However, despite their promising performance, the high costs and technical challenges associated with ILs highlight the necessity for alternative approaches that offer comparable

^a Faculty of Engineering and Natural Sciences, Sabanci University, Tuzla 34596, Istanbul, Turkiye

^b ILKO, Sancaktepe 34885, Istanbul, Turkiye

^c Sabanci University Nanotechnology Research and Application Center (SUNUM), Tuzla 34596, Istanbul, Turkiye

^{*} Corresponding author at: Faculty of Engineering and Natural Sciences, Sabanci University, Tuzla 34596, Istanbul, Turkiye. E-mail address: nur.mustafaoglu@sabanciuniv.edu (N. Mustafaoglu).

efficacy while being cost-effective for both research and clinical applications (Bernard-Arnoux et al., 2016).

Niosomes have emerged as a viable alternative to liposomes due to their lower production costs, enhanced stability, biocompatibility, and reduced toxicity (Bartelds et al., 2018a; De et al., 2018; Gharbavi et al., 2018; Ibrahim Bekraki, 2020; Kazi et al., 2010; Khoee and Yaghoobian, 2017; Liga et al., 2024). Compared to liposomes, niosomes exhibit higher water permeability and greater mobility of head groups, making them favorable candidates for drug delivery applications (Bartelds et al., 2018). Although the term "immunoniosomes" (INs) is introduced in this study, previous research has investigated antibody conjugation to niosomes, primarily by targeting thiol functional groups on antibodies following their reduction (Liu et al., 2017) and using maleimide functionalized quantum dots (Saharkhiz et al., 2024).

In this study, we present novel methods for conjugating whole antibodies and Fab fragments to niosomes using two distinct approaches (Fig. 1): (i) A novel linker containing an indole ring structure, which binds moderately to a conserved nucleotide binding site (NBS) on the variable regions of the antibodies and Fab fragments. This site-specific covalent conjugation is achieved through UV activation, employing a technique termed UV-NBS (Mustafaoglu et al., 2017; Mustafaoglu et al., 2015a, 2015b). (ii) Carboxylated niosomal nanoparticles, to which antibodies or Fab fragments are conjugated through their primary amine groups on the lysine sidechains using EDC/NHS chemistry.

To the best of our knowledge, this is the first study to apply the UV-NBS conjugation approach to lipid-based nanoparticles, including niosomes. While UV-NBS chemistry has previously been used for surface immobilization and other biomolecular applications, its translation to nanocarrier platforms represents a novel advancement. This approach enables mild, site-specific conjugation conditions that preserve antibody functionality—an essential feature for therapeutic efficacy. Furthermore, we present a direct comparison between Fab and full-length mAb conjugation efficiencies using both UV-NBS and EDC/NHS strategies on niosomal formulations. This comparative analysis provides mechanistic insights into how conjugation chemistry influences targeting performance, stability, and potential therapeutic applicability—contributing new knowledge to the field of antibody-functionalized drug delivery systems.

Bevacizumab, an FDA-approved monoclonal antibody (mAb) targeting vascular endothelial growth factor (VEGF), was selected for the formulation of INs (Cohen et al., 2009; Garcia et al., 2020). Initially, approved for the treatment of colon cancer, Bevacizumab has been repurposed for various cancer types, including lung, ovarian, and renalcell carcinoma, under the brand name of Avastin® (2004) (Garcia et al., 2020; Schmidt et al., 2012). More recently, it has been approved for treating recurrent glioblastoma multiforme (GBM) due to its enhanced penetration into the central nervous system (CNS) and superior efficacy compared to other antibody candidates (Arevalo et al., 2019; Gil-Gil et al., 2013). Although the downstream signaling mechanism of Bevacizumab remain unclear, its clinical success in GBM treatment is well established (Arevalo et al., 2019; Gil-Gil et al., 2013b; Weathers et al., 2016). Enhancing Bevacizumab's blood circulation time through nanocarrier integration has demonstrated significant potential for improving GBM treatment outcomes (Narsinh et al., 2024; Reverberi and Reverberi, 2007).

To evaluate this approach, we tested Bevacimab (or its biosimilar)-conjugated niosomes in the GBM cell line U87, which overexpresses VEGF, and in human umbilical vein endothelial cells (HUVECs), representing normal VEGF expression. This work demonstrates the conjugation of both mAbs and their Fab fragments onto niosomal formulations. Fab fragments, compared to full mAbs, offer advantages such as lower molecular weight, reduced immunogenicity, faster antigen binding, and potentially improved tumor-suppressive efficacy (Bordeau and Balthasar, 2021; Chiu et al., 2019; Merino et al., 2018; Wiwatchaitawee et al., 2021). However, Fab fragments face challenges, including shorter blood circulation time and quicker renal clearance relative to mAbs (Selis et al., 2016). By integrating Fab fragments with niosomes, these limitations can be mitigated, extending their blood circulation time while maintaining antigen-binding efficiency, facilitated through site-specific conjugation methods.

Consequently, in this study, we generated mAb- and Fab-conjugated niosomes and referred them as Nio-mAb and Nio-Fab, respectively. Combining Fab fragments with nanoparticles provides additional benefits, advancing drug delivery strategies and broadening the range of effective therapeutic applications (Lim and Ma, 2019; Rong et al., 2022). The integration of mAbs or Fab fragments with niosomes represents a

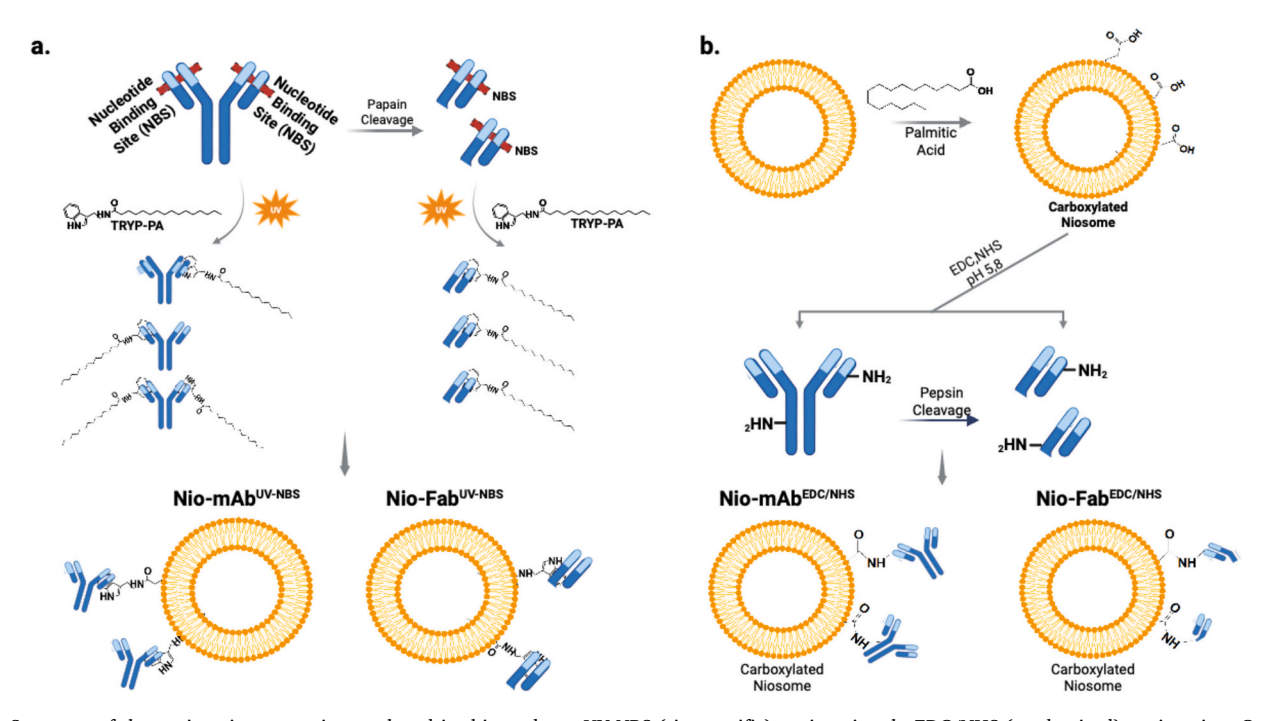


Fig. 1. Summary of the conjugation strategies employed in this study. a. UV-NBS (site-specific) conjugation; b. EDC/NHS (randomized) conjugation. Created in BioRender. Cakir et al. (2024) https://BioRender.com/i69f064

promising strategy for developing safe and effective alternatives to traditional antibody-based therapies for cancer treatment. Furthermore, this approach has the potential to expand the utility of antibody- and Fab fragment-conjugated niosomes to other fields, including immunotherapy, infectious disease treatment, and neurodegenerative disorder management, where precise therapeutic agent delivery is critical.

2. Method & materials

2.1. mAb and Fab preparations and characterization

Papain enzymatic cleavage was performed to obtain Fab fragments, and a Protein A affinity column was employed to capture and purify them. The original mAb (Avastin®) was generously provided by ILK-OGEN (serial number: 10011363253619). A biosimilar mAb from ILK-OGEN's preclinical Protein A output was utilized for all method optimizations due to its higher concentration and larger volume. It is important to emphasize that although all method optimizations were conducted using the in-process Bevacizumab biosimilar, the final results reported throughout this paper were obtained with the original Bevacizumab. For purification, the Pierce Fab Preparation Kit (Thermo Fisher, USA) was employed. After purification, a desalting spin column (Thermo Fisher, USA) was used to exchange the formulation buffer (50 mM sodium phosphate buffer at pH 6.2, 60 mg/mL α,α-trehalose dihydrate, and 0.4 mg/mL polysorbate 20). Additionally, 30 kDa molecular weight cut-off filters (Merck, Germany) were employed to isolate the Fab fragments from the formulation buffer and concentrate them. The purity and size of the mAb and Fab fragments were assessed using SDS-PAGE (Fig. S1a). The sizes of the Fab and mAb fragments were compared between the biosimilar and original products using DLS analysis (Fig. S1b and S2c).

2.2. Tryptamine-Palmitic Acid (TRYP-PA) linker synthesis

To synthesize TRYP-PA linker, EDC/NHS chemistry was used between the palmitic acid and tryptamine molecule (Fig. S4). EDC (1-ethyl-3-(3-dimethylaminopropyl)carbodiimide hydrochloride, Fisher, USA) and NHS (N-hydroxysuccinimide, Thermo Fisher, USA) were prepared as 10 mM stock solutions in activation buffer. The activation buffer consisted of 0.1 M MES (2-[N-morpholino]ethanesulfonic acid, BupH™ MES buffer saline packs, Thermo Fisher, USA) with 0.5 M NaCl, adjusted to pH 6.0. Tryptamine (Sigma-Aldrich, Germany) was dissolved in activation buffer at a concentration of 1 mg/mL. EDC and NHS were simultaneously added to the tryptamine solution at final concentrations of 2 mM and 6 mM, respectively. The reaction mixture was incubated with continuous shaking for approximately 15 min. To quench the reaction, BME (2-mercaptoethanol, Gibco, USA) was added to achieve a final concentration of ~20 mM. Excess reducing agents and unreacted crosslinkers were removed using PBS-equilibrated Zeba Spin Desalting Columns (Thermo Scientific, USA). Palmitic acid (Sigma-Aldrich, Germany) was prepared at an equimolar concentration to tryptamine (1 mg/mL) in coupling buffer. The coupling buffer consisted of PBS supplemented with 100 mM sodium phosphate (Sigma-Aldrich, Germany) and 150 mM NaCl (Sigma-Aldrich, Germany), adjusted to pH 7.2. The prepared palmitic acid solution was added to the tryptamine solution, and the reaction was allowed to proceed for 2-3 h to ensure complete coupling. To terminate the reaction, 50 mM Tris-base was added, followed by buffer exchange with PBS (pH 7.2) using desalting spin columns. High-performance liquid chromatography (HPLC) (Waters, USA) and Fourier transform infrared spectroscopy (FTIR) (Thermo Fisher, USA) were employed for the purification and characterization of the TRYP-PA linker. HPLC analysis was performed using a photodiode array (PDA) detector mode. A C18 reverse-phase chromatography column (Agilent, USA) with an inner diameter (ID) of 4.2 mm, a length of 80 mm, and a particle size of $5 \mu m$ was used for all analyses. The optimized gradient conditions are provided in Supplementary Table 3. Widespectrum of UV screening (210–550 nm) was applied to determine possible impurities and PDA detector was used to perform this screening.

2.3. Generation of INs using UV-NBS conjugation

2.3.1. Conjugation of TRYP-PA linker with mAb/Fab using UV-NBS method

To achieve site-specific conjugation of the TRYP-PA linker to the conserved NBS region of mAb/Fab, UV exposure for a defined duration and intensity was required, as reported in a previous study (Alves et al., 2013b). The measurements and calculations for UV exposure are detailed in the *supplementary information* and *Fig. S5*. For sample preparation, 300 nM TRYP-PA linker, dissolved in 0.2 µm filtered sterile water, was mixed in equimolar amounts with mAb/Fab in amber tubes and incubated for 30 min in the dark at room temperature. Following incubation, test groups were exposed to UV for varying time intervals.

To test the antigen-binding activity of UV-conjugated antibodies, high-binding 96-well ELISA plates (Corning, USA) were coated with VEGF (100 ng/mL per well) and used for the ELISA assay. For cellular binding analysis, U87 and HUVEC cell lines were seeded at a density of 7500 cells/well in 24-well plates, in a replicate volume of 500 µL. Approximately 6.0×10^6 cells were required per cell line, and they were seeded one day before the assay. Pre-optimized mAb/Fab dilution factors (1:400 and 1:800, respectively) were used for cell seeding. After a 2h incubation at 37 °C in the dark, FITC-tagged anti-mouse secondary antibody (Jackson ImmunoResearch, USA), diluted in starvation media, were added to the wells. Following an additional 2-h incubation under the same conditions, the media were removed, and cells were collected on ice using a cell scraper in DPBS (-/-). The collected cells were fixed with 0.1 % paraformaldehyde (PFA) and stored at 4 °C for a maximum of five days before analysis. Samples were run in a flow cytometry and the obtained results were analyzed using FlowJo, with intersections between controls and test groups subtracted for data interpretation.

2.3.2. Insertion of TRYP-PA conjugated mAb/Fabs into niosomes

TRYP-PA linkers were conjugated to the NBS region of the mAb or Fab through an 8-min UV exposure following a 30-min pre-incubation in the dark. Two insertion strategies, thin-film hydration and freeze-thaw, were employed to incorporate the linker-conjugated mAb/Fab into niosomes. The development of alternative insertion methods was necessary due to processing challenges, such as the high glass transition temperature (~60 °C) and sonication, both of which are known to accelerate mAb degradation. The thin-film hydration method was optimized by adjusting the water bath temperature to 37 °C and performing ice-cold sonication. The linker-conjugated mAb/Fab was incorporated at 0.5 % of the total volume in chloroform. Span 60, Tween 80, and cholesterol were prepared according to the compositions detailed in Table 1. A rotary evaporator was used, starting at 400 psi and gradually decreasing to 60 psi over 30 min. The resulting thin films were incubated overnight in a desiccator, hydrated with an equal volume of PBS, and subjected to ice-cold sonication for approximately 30 min. For the freeze-thaw method, pre-formed unloaded niosomes were mixed with the linker-conjugated mAb/Fab at the final concentrations specified in Table 1, with a TRYP-PA linker content of 0.5 % (ν /v) for mAb/Fab. The mixture was incubated at room temperature for 15 min, followed by freezing at -20 °C. This cycle was repeated four times at four-hour intervals.

The obtained results are presented in Fig. S6. Additionally, the cellular binding profiles of UV-NBS generated INs (Nio^{UV-NBS}) prepared using both techniques were evaluated using U87 cells via flow cytometry, with the results shown in Fig. S7.

Table 1The unconjugated niosome formulation content was selected based on a previously optimized cell-based research study.(Cakir et al., 2024).

Formulation ID	Ingredients	Ratio (%)	Final Concentration (mM)	Processing
Nio-1	Cho: S60: T80	48:49:03	0,13	Gradient Vacuum, Fixed sonication (90 mins)
Nio-2	Cho: S60: T80	50:50:00	0,1	Gradient Vacuum, Fixed sonication (90 mins)
Nio-3	Cho: S60: T80	50:50:00	0,1	Gradient Vacuum, Fixed sonication (45 mins)
Nio-4	Cho: S60: T80	50:50:00	0,2	Gradient Vacuum, Fixed sonication (90 mins)

2.4. Generation of INs using EDC-NHS conjugation

2.4.1. Preparation and characterization of PA-incorporated niosomes

To conjugate mAb/Fab with niosomes using the EDC/NHS conjugation strategy, niosomes were formulated with palmitic acid (PA) to introduce carboxylic acid groups on their surface. The PA concentration was kept the same as the TRYP-PA linker used in the UV-NBS conjugation strategy, i.e., 300 nM in ethanol. Nio-1, Nio-2, Nio-3, and Nio-4 niosome formulations, with four different PA load percentages (0.1 %, 0.25 %, 0.5 %, and $1 \% \nu/\nu$), were prepared by the thin-film hydration method using chloroform (Merck, Germany) as the organic solvent. The final concentrations and content of the niosome formulations are presented in Table 1. Using a rotary evaporator with a gradient vacuum program, the dried milky layers were hydrated with PBS at pH 7.4 and then filtered through 0.2 µm sterile filters after moderate sonication. DLS (Malvern Zeta Sizer 3000, USA) analysis was performed on the PAloaded niosomes, which were diluted 1:10 in PBS(-/-), which lacks calcium and magnesium ions. Although PBS(-/-) at pH 7.4 may influence zeta potential measurements due to its ionic strength, it was selected to reflect physiological conditions relevant to the intended application of INs. To ensure consistency and avoid measurement artifacts, PBS(-/-) was also used as the blanking solution. The size (nm), PDI, and zeta potential (mV) for each PA loading percentage are shown in Fig. S8. The desired physicochemical properties were graphed and analyzed using GraphPad Prism. The encapsulation efficiency (EE%) of PA-loaded niosomes was not calculated. The maximum load was inferred from the proportional increase in surface negative charge, which corresponded to the higher PA load percentage.

2.4.2. Conjugation of mAb/Fab on PA-loaded niosomes using EDC/NHS chemistry

mAb/Fab were prepared at three different concentrations: 0.05 mg/mL, 0.1 mg/mL, and 0.2 mg/mL (Fig. S9). For the coupling reaction, both activation and coupling buffers were prepared. The activation buffer consisted of 0.1 M MES and 0.5 M NaCl at pH 6.0, while the coupling buffer was PBS (Sigma-Aldrich, Germany) with 100 mM sodium phosphate (Sigma-Aldrich, Germany) and 150 mM NaCl (Sigma-Aldrich, Germany) at pH 7.2. Stock solutions of 10 mM EDC and NHS were prepared in the activation buffer. mAb/Fab were dissolved in the coupling buffer. Thin films of niosomes (Table 1) containing PA were obtained by drying at 60 °C. The concentration of dried PA-loaded niosomes was maintained at 1 mg/mL, and they were dissolved in the activation buffer to a final concentration of 1 mg/mL. EDC and NHS were added to the PA-loaded niosomes to achieve final concentrations of 2 mM and 6 mM, respectively, and the mixture was incubated for 15

min. The reaction was quenched with cell culture-grade BME (2-mercaptoethanol) (Gibco, USA) and subsequently processed using a Zeba desalting column (Thermo Fisher, USA). Different mAb/Fab concentrations in the coupling buffer were then added to the activation buffer mixture. After a 2-3 h incubation, the reaction was stopped using 50 mM Tris-base. The INs generated by EDC-NHS conjugation (Nio EDC/NHS) were desalted by spin column and exchanged into PBS at pH 7.2. Physicochemical analysis was performed using DLS, and the size, polydispersity index (PDI), and zeta potential (mV) were measured. The desired ranges were a size between 100 and 200 nm, PDI between 0.2 and 0.5, and zeta potential between -10 and 10 mV. The results obtained for the different mAb/Fab concentrations in INs were analyzed using GraphPad Prism for statistical evaluation and graphing. Statistical size comparisons between mAb/Fab conjugated Nio EDC/NHS formulations (Fig. S9) compared to their corresponding non-conjugated counterparts (Fig. S8) were provided in Supplementary Tables 11 to 14 for mAb and Fab conjugations, respectively.

2.4.3. Determination of Encapsulation Efficiency (EE%) of UV-NBS INs

To determine the encapsulation efficiency (EE%) of the IN formulations, a standard curve for mAb and Fab was first constructed to predict the concentration of the protein of interest. Five different concentrations of mAb and Fab (0.01 mg/mL, 0.05 mg/mL, 0.1 mg/mL, 0.125 mg/mL, and 0.2 mg/mL) were prepared in formulation buffer. The absorbance of these solutions was measured using a Nanodrop A280 (Thermo Fisher, USA), with the formulation buffer blanked at 280 nm, as shown in Fig. S11d and Fig. 11e.

To release the encapsulated protein from UV-NBS INs, each IN formulation was centrifuged at 15000 rpm for 15–20 min. The supernatant was collected in separate sample tubes, and absorbance was measured using the Nanodrop A280. The protein absorbances of the supernatants were used in the equation derived from the standard curve to calculate the unknown protein concentration. The released protein concentration was determined by the difference between the known protein concentration initially loaded into the IN formulations and the measured protein concentration in the supernatant. The EE% for each IN formulation was then calculated using the equation below (Eq. 1).

$$EE\% = \frac{Amount \ of \ drug \ encapsulated}{Total \ amount \ of \ drug \ added} \times 100 \tag{1}$$

2.4.4. Determination of percent conjugation efficiency (CE%) of ${\rm Nio}^{\rm EDC/}$ NHS formulations

In the EDC/NHS formulation of INs, the niosomes are carboxylated with palmitic acid by loading 0.5 % TRYP-PA into each niosome formulation, after which mAb/Fab antibodies are conjugated to the carboxylated niosomes. To calculate the conjugation efficiency (CE%), the absorbance of the initial solution before conjugation is measured using UV-visible spectroscopy at a wavelength of 280 nm. Antibodies, in the same reaction volume, concentration, and solution, are added to the reaction without PA-loaded niosomes (prior to conjugation) and their absorbance at 280 nm is recorded. This absorbance value is used in the equation derived from the standard curve of mAb/Fab to calculate the antibody concentration. Subsequently, the EDC/NHS reaction is performed by activating the PA-loaded niosomes, followed by amine coupling. The same absorbance measurement is then repeated, blanking the absorbance of only PA-loaded niosomes at 280 nm. The antibodies from the initial reactant amount and the antibody concentration after the EDC/NHS reaction in IN forms are used to calculate CE%. The same calculation is performed for the absorbance value obtained postconjugation. The equation is given below as Eq. 2.

$$CE\% = \left(\frac{Conjugated\ Antibody}{Total\ Antibody\ Added}\right) \times 100 \tag{2}$$

2.4.5. Cellular uptake and cellular binding profiles of original and biosimilar mAb/Fab

Prior to linker synthesis and subsequent conjugation, the cellular binding and uptake responses of both the biosimilar and original Bevacizumab mAb and Fab therapeutics were evaluated. These assays were conducted under the previously optimized conditions (Detailed protocols were provided in supplementary information and Fig. S1, S2, and S3). The results presented in Fig. S1d were derived from the signals obtained during this analysis. Furthermore, statistical analyses were performed to assess potential differences in binding and uptake between the original and biosimilar therapeutics. Identifying these differences was crucial for advancing the optimization studies using the biosimilar product. Supplementary Tables 1 and 2 summarize the statistical comparisons of the biosimilar and original mAb and Fab in both cell lines. One-way ANOVA was employed for the statistical evaluations.

2.4.6. Cellular uptake and binding of mAb/Fab-loaded INs

The HUVEC and U87 cell lines were utilized to evaluate the cellular uptake and binding performance of UV-NBS and EDC/NHS-modified INs. Two detection strategies were employed to assess cellular responses of the INs using flow cytometry assay. The first strategy involved using FITC-tagged secondary antibodies to detect INs via secondary antibody binding. The second strategy involved developing FITC-loaded INs to eliminate potential interference in secondary antibody binding. The amount of FITC loading on INs was determined based on previous optimization studies conducted with the sole niosomal formulation (Fig. S10 and Fig. S11).

In the first strategy, UV-NBS and EDC/NHS-conjugated INs were prepared, and their physicochemical properties were assessed by DLS prior to the binding and uptake assays. Freshly prepared INs were stored for one day at 2–8 $^{\circ}$ C. Concurrently, U87 and HUVEC cells were seeded at 7500 cells/well in 24-well plates, with triplicates for each mAb/Fabconjugated niosome formulation. A total of 6×10^6 cells were required for each assay from each cell line, ensuring 7500 cells in 500 μL . INs containing mAb and Fab formulations were diluted in starvation media to 1:400 and 1:800, respectively, and added to wells at 100 µL per well. For the uptake analysis, INs were allowed to incubate for 4 h to allow for complete uptake, followed by 2 h for FITC-tagged antibody binding. After incubation, media were removed, and cells were washed three times with DPBS (-/-). Cells were detached using trypsin (Gibco, USA) and neutralized with growth medium after 5 min of incubation at 37 °C. The cells were collected in individual sample tubes. The tubes were centrifuged at 2000 rpm for 5 min, and the pellets were resuspended in 2 mL of DPBS (-/-) with 0.1 % PFA for fixation of the cells. In the binding analysis, the same assay was performed on ice, and instead of the trypsinization step, the cells were collected using a cell scraper. The samples were then analyzed by flow cytometry (BD Fortessa, USA) and processed using FlowJo software. Control groups included cells without treatment, cells treated with only the secondary antibody, and cells treated with Nio-1, Nio-2, Nio-3, and Nio-4 formulations or mAb/Fab alone, which were prepared as described for the INs.

In the second strategy, niosomal formulations were tagged with 0.05 % FITC (Fig. S10 and Fig. S11). The physicochemical properties of the FITC-tagged INs were assessed by DLS after dilution (1:100) in PBS. The FITC-tagged INs were stored for one day at 2–8 °C in a dark environment. HUVEC and U87 cells were seeded and treated as in the first strategy, excluding the secondary antibody. FITC-tagged mAb/Fab INs were diluted 1:400 and 1:800 and added to the wells at 100 μ L. Uptake assays were performed with a 4-h incubation, while binding assays involved a 2-h incubation. Cells were processed in the same manner as in the first strategy, and samples were analyzed by flow cytometry (BD Fortessa, USA) and the data were processed using FlowJo.

Additionally, IN loaded cells, both U87 and HUVEC, were imaged under fluorescence microscopy (*Fig. S12*). INs inside of the cells were captured by FITC-tagged secondary antibody (Jackson Immuno Research, USA). The cells were stained with DAPI (1:1000 dilution) after

fixation of cells by 1 % PFA (Sigma-Aldrich, Germany) to visualize the cellular nucleus.

2.4.7. Assessing the cytotoxicity of INs on cells

To determine the toxicity of Nio-mAb/Fab^{UV-NBS} and Nio-mAb/ lium bromide (MTT) (Neofroxx, Germany) assay was performed. A 0.5 mg/mL MTT solution was prepared in filtered PBS using a 0.2 µm sterile filter. U87 and HUVEC cells were seeded into a 96-well plate (ISOLAB, Germany) at a density of 10,000 cells/well, calculated based on the media volume corresponding to each cell line (DMEM and RPMI 1640, respectively). The cell-containing media solutions were evenly distributed in a sterile petri dish (ISOLAB, Germany) before being seeded into the plates, with mixing performed 3-4 times using a multi-channel pipette. The cells were incubated overnight before the assay. Four different concentrations of each IN were prepared: 0.15 mg/mL, 0.015 mg/mL, 0.0015 mg/mL, and 0.00015 mg/mL. All dilutions were made in starvation media (without fetal bovine serum, FBS). A 24-h exposure time was set for toxicity assessment. To compare the original therapeutic dosage to the cytotoxicity assay results, the dilution factor equation (2)

$$Dilution Factor = \frac{Original \ Concentration}{Diluted \ Concentration}$$
(3)

The original Bevacizumab concentration was 25 mg/mL. The highest concentration of INs used in this toxicity assay was 0.15 mg/mL. Using Eq. 3, the exposed dosage in this assay was 166.67 times more diluted than the original in 2D. After 24 h of exposure to the INs, MTT was added to each well and incubated for 3–4 h. Following the MTT incubation, the solutions in the wells were removed, and a sodium dodecyl sulfate (SDS)-based solubilization solution containing 10 % SDS (w/v) (Sigma-Aldrich) and 0.01 M HCl (Sigma-Aldrich) prepared in distilled water was added. The wells were incubated for 30 min, and absorbance was measured at 570 nm using a plate reader (ThermoFisher, USA). Each plate included triplicates of each IN dilution, with the results normalized to control wells containing cells with no exposure. The obtained absorbance values were normalized using the following equation to calculate cellular viability (%) (Eq. 4).

$$\textit{Cellular Viability (\%)} = \frac{\textit{Measured Absorbance} \times 100}{\textit{Max (All Measured Absorbance Series)}} \tag{4}$$

Cellular viability percentages were graphed against the logarithmic molarity (log[M]) of IN concentrations, and sigmoidal 4PL nonlinear regression analysis was applied in GraphPad Prism. Control groups, including biosimilar and original mAb/Fab, were prepared, exposed, and analyzed simultaneously with the experimental groups.

3. Results & discussion

3.1. Conjugation of TRYP-PA linker to mAb/Fab via UV-NBS method

To successfully incorporate monoclonal antibodies (mAbs) and Fab fragments into niosomal formulations without compromising their antigen-binding activities, these biomolecules were first conjugated with palmitic acid (PA) groups via their conserved nucleotide-binding site (NBS) region using the previously described UV-NBS method (Alves et al., 2014, Alves et al., 2012, Alves et al., 2013a; Mustafaoglu et al., 2017). For this conjugation, PA was coupled with a ring-structured tryptamine molecule, which has an affinity for the NBS (Alves et al., 2013a; Mustafaoglu et al., 2017), to serve as a site-specific linker for mAbs and Fab fragments. Consequently, the TRYP-PA linker was synthesized (*Fig. S4*) and purified (Fig. 2). The purity of the linker was assessed using high-performance liquid chromatography (HPLC) (Fig. 2b), revealing a purity of >95 %. The lyophilized form of TRYP-PA was further characterized using fourier-transform infrared (FTIR) spectroscopy (Fig. 3a). PA (1) and tryptamine (2) were used as controls to

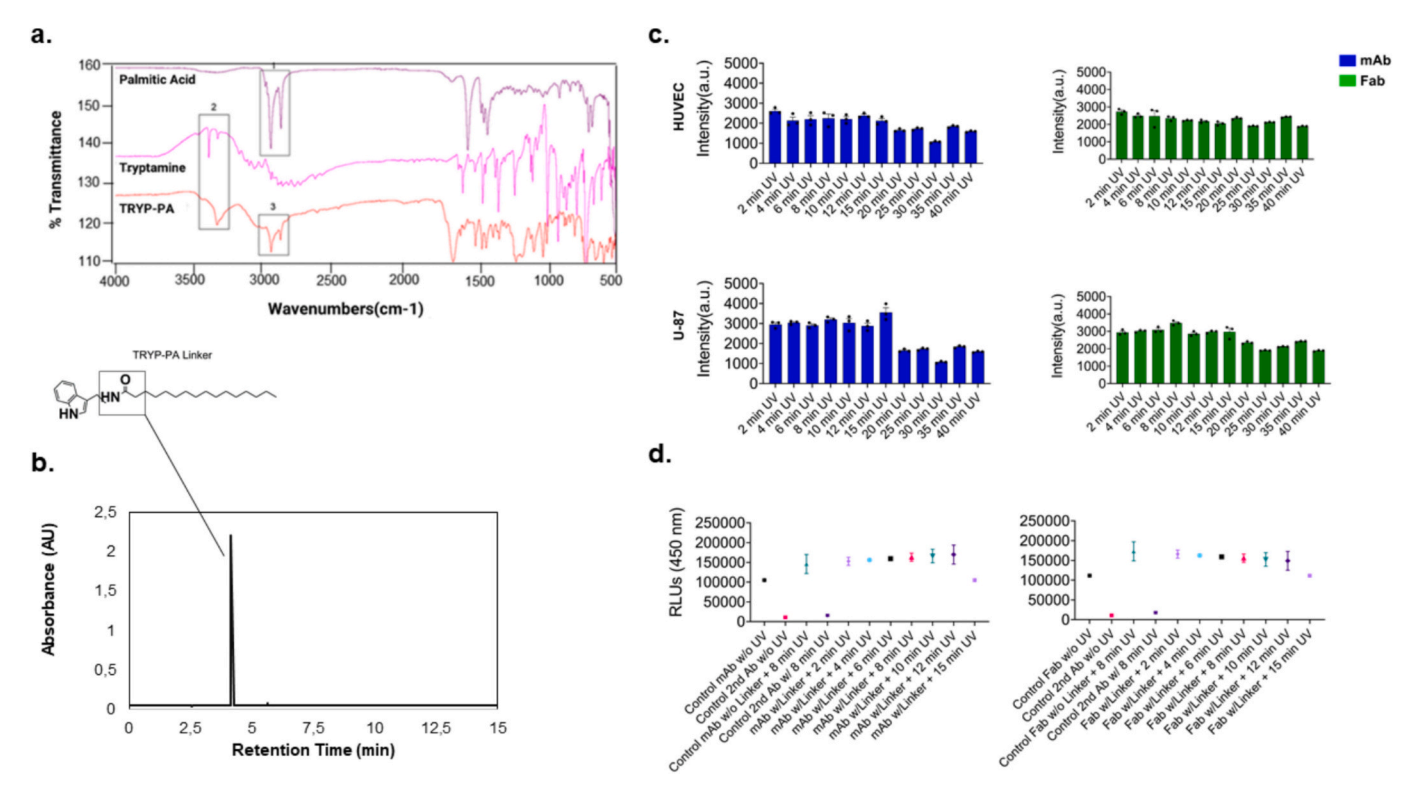


Fig. 2. Conjugation of TRYP-PA to mAb and/or Fab using the UV-NBS method. a. FTIR spectrum of the synthesized TRYP-PA linker. b. RP-HPLC chromatogram of the TRYP-PA linker, determined using a PDA detector at an absorbance of 220 nm. c. Antigen-binding activities of mAb and Fab structures after varying durations of UV exposure (365 nm), assessed by flow cytometer in HUVEC and U87 cell lines. d. Structural integrity of mAb and/or Fab structures following UV exposure, evaluated using direct ELISA.

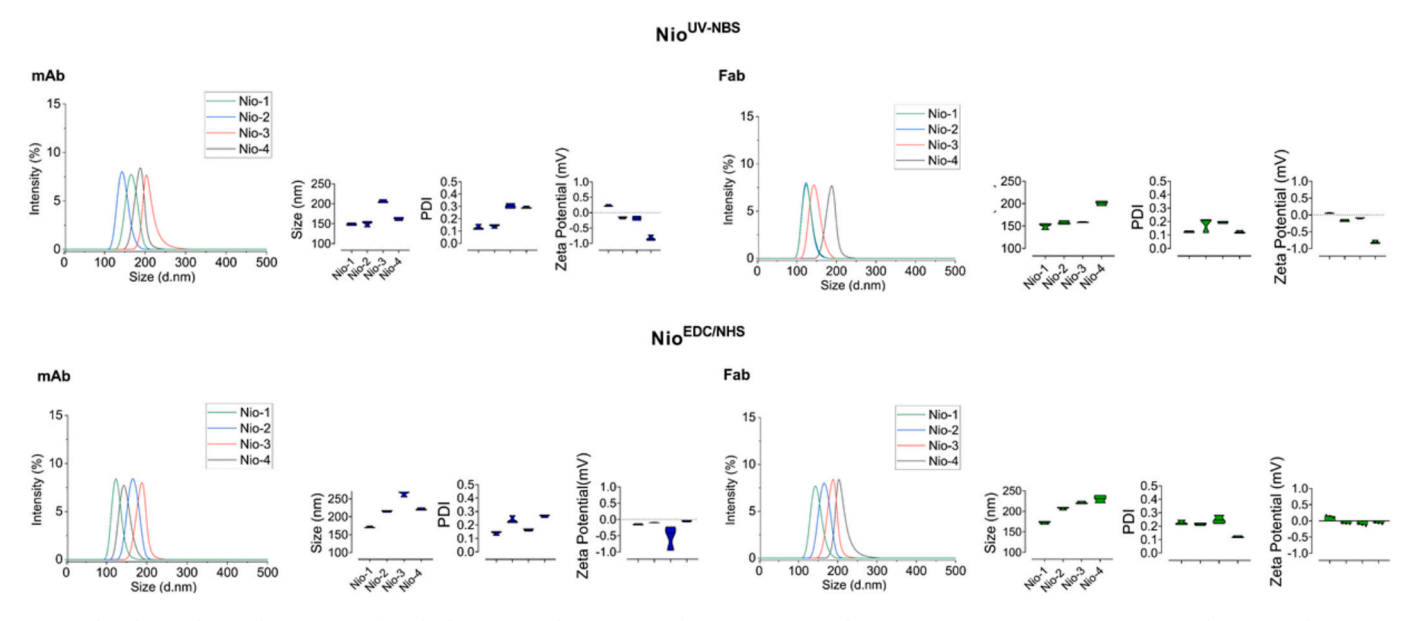


Fig. 3. The physicochemical properties of antibody-conjugated INs, prepared using UV-NBS and EDC/NHS conjugation strategies, were characterized using DLS measurements.

evaluate chemical composition changes following the conjugation of tryptamine and PA (3). As shown in Fig. 2a, the spectra of (1) and (3) exhibited strong O—H bending vibrations, typically observed in the range of $1300-1440~{\rm cm}^{-1}$. Additionally, the spectra of (2) and (3) displayed strong N—H stretching vibrations, characteristic of amine groups, typically found in the range of $3300-3500~{\rm cm}^{-1}$.

The site-specific conjugation of the synthesized TRYP-PA linker to mAbs and Fab fragments was facilitated by UV exposure, enabling

covalent binding of the indole-containing molecule, tryptamine, to the NBS regions of mAbs/Fab, as illustrated in Fig. 1. Previous studies have reported that the optimal UV intensity and wavelength for conjugating tryptamine via the NBS region is approximately 1–2 J/cm² at 254 nm (Mustafaoglu et al., 2017; Mustafaoglu et al., 2015a). In this study, a UV wavelength of 365 nm was used, and the exposure time was optimized to ensure effective crosslinking while preserving the antigen-binding site and structural integrity of the antibody. Detailed calculations based on

Planck's law, used to achieve the required energy of 1 J/cm^2 per unit area within a specific timeframe, are provided in the Supplementary Information (*Fig. S5*). Based on these calculations and intensity measurements, achieving an approximate UV intensity of 1 J/cm^2 required 8 min of exposure at 365 nm.

To evaluate the effect of UV exposure on the antigen-binding activity of Fab and mAb following conjugation with the TRYP-PA linker, flow cytometry experiments were performed using HUVEC (healthy) and U87 (glioblastoma) cells. These cell lines were selected based on their demonstrated binding and uptake of Bevacizumab and its biosimilar counterpart, as shown in Fig. S1d. As illustrated in Fig. 2c, the results indicate that the antigen-binding activity of TRYP-PA-conjugated mAbs remained unaffected by UV exposure for up to 12 min; however, beyond this point, disruptive effects of UV exposure on binding activity became apparent. Although the effect on Fab-linker conjugates was less pronounced, a clear trend of decreasing binding activity was observed with increasing UV exposure duration. These findings are consistent with previous reports (Alves et al., 2013b; Reinmuth-Selzle et al., 2022). Based on these results, it was determined that an optimal protocol involves incubating the linker and antibody in the dark for 30 min, followed by 8–12 min of UV exposure. This exposure time was sufficient for linker conjugation while preserving the antigen-binding activity of Fab

Additionally, to validate the cell-based assay results, the antigenbinding activity and structural stability of linker-conjugated Fab and mAbs were assessed under varying UV exposure conditions using VEGFcoated ELISA plates. While cellular binding assays provide physiologically relevant data (Fig. 2c), this ELISA-based approach ensured a controlled experimental setup by eliminating variability in antigen expression levels. Specifically, each well was coated with a consistent amount of VEGF (100 ng/mL per well), allowing for a direct evaluation of antigen-binding activity. Although a difference was observed between antibodies exposed to UV energy; the presence of the linker did not affect the effect of UV exposure on structural integrity of either Fab fragments or mAbs, as demonstrated in Fig. 2d. However, the binding signal diminished after 12 min of UV exposure, a trend consistent with the in vitro cell-binding assay results (Fig. 2c). Based on these findings, an 8-min UV exposure (~1 J/cm²) was selected for conjugating the TRYP-PA linker to mAbs and Fabs in subsequent experiments.

3.1.1. Incorporation of TRYP-PA conjugated mAb/Fab into niosomes (NiomAb $^{UV-NBS}$) and Nio-Fab $^{UV-NBS}$)

The UV-NBS conjugated mAb and Fab were incorporated into INs using two different strategies for antibody-linker conjugation: (i) thin-film hydration and (ii) freeze-thaw. These two approaches were selected due to the potential challenges associated with thin-film hydration, as its process conditions—particularly elevated water bath temperatures required to reach the glass transition temperature ($\sim 60~^\circ$ C)—may accelerate protein degradation. Additionally, direct vacuum application could lead to the loss of drug components, while the use of organic solvents might induce forced degradation of mAbs and Fabs.

In the first strategy, previously optimized conditions for site-specific linker-antibody conjugation were employed, followed by encapsulation via the thin-film hydration technique. To overcome the limitations of this method, the process was adapted to achieve the desired Nio^{UV-NBS} forms. Specifically, after the linker-conjugated mAb/Fab was prepared, the same loading percentage as in PA-loaded niosomes (0.5 %) was dissolved in chloroform. The chloroform was then immediately removed using a dry nitrogen stream and subjected to rotary evaporation. This step minimized prolonged exposure of the linker-conjugated mAb/Fab to organic solvents, reducing the risk of degradation. During rotary evaporation, vacuum pressure was gradually decreased while maintaining a water bath temperature of 37 °C to prevent heat-induced degradation.

In the second strategy, the freeze-thaw method, previously used for

FITC loading into niosomes,(Cakir et al., 2024) was adapted for the incorporation of TRYP-PA conjugated mAbs and Fabs into niosomes after their formation. For this purpose, four different niosome formulations and linker-conjugated mAbs and Fabs were prepared separately. The two components were then gently mixed using a horizontal shaker and incubated at room temperature for 30 min to ensure uniform distribution. Subsequently, periodic freeze-thaw cycles were applied by instant freezing at $-20\,^{\circ}\text{C}$ followed by thawing at RT, allowing passive insertion of the linker-conjugated mAbs and Fabs into the niosome formulations. Excess unbound antibody-linker conjugates were removed using a 30 kDa Amicon ultrafiltration unit (Merck) and Ab/Fab conjugated niosomes were filtered through 0.2 μm sterile filter before cellular experiments.

The Nio UV-NBS formulations obtained from both the thin-film hydration and freeze-thaw strategies were analyzed using dynamic light scattering (DLS) to assess their physicochemical properties (*Fig. S6*). The expected size range was between 100 and 200 nm, with a near-neutral zeta potential and a polydispersity index (PDI) between 0.2 and 0.5, as shown in *Fig. S6*. Although Nio UV-NBS formulations generated by freeze-thaw strategy exhibited enhanced physicochemical properties, particularly in particle size, their cellular binding profiles were evaluated in U87 cells alongside thin-film hydrated IN formulations (*Fig. S7*). However, complete success could not be claimed due to the need for further optimization of the freeze-thaw method.

As with other conjugation strategies, the freeze-thaw approach can be refined by adjusting the antibody or linker-conjugated antibody concentration, as well as the number of freeze-thaw cycles. Further optimization of these parameters could establish this method as a viable alternative to thin-film hydration for future studies. The optimized conditions for Nio^{UV-NBS} (INs generated via UV-NBS conjugation) were analyzed using DLS in parallel with Nio^{EDC/NHS} (INs generated via EDC/NHS chemistry) and are reported in Fig. 3.

3.1.2. Generation of INs via EDC/NHS chemistry (Nio-mAbEDC/NHSand Nio-FabEDC/NHS)

To conjugate mAb and Fab onto niosomes using EDC/NHS chemistry, carboxyl functionalization of the niosome formulations was first achieved by incorporating PA. Four different niosome formulations (Nio-1, Nio-2, Nio-3, and Nio-4, as shown in Table 1) were used to introduce carboxyl groups, enabling their coupling with the amine groups of lysine side chains in mAbs and Fabs via EDC/NHS chemistry (schematized in Fig. 1). The target physicochemical properties were a particle size of 100-200 nm, a PDI between 0.2 and 0.5, and a zeta potential ranging from -10 to +10 mV to enhance tissue barrier penetration and efficacy. These preset physicochemical conditions were a key criterion for optimization (Cakir et al., 2024). A primary consideration was determining the optimal PA loading percentage for niosome functionalization. To this end, four different PA loads (0.1 %, 0.25 %, 0.5 %, and 1 %) were evaluated, and their physicochemical properties were analyzed using DLS, as shown in Fig. S8. The results indicated that all PA-loaded niosome formulations fell within the desired size (100-200 nm) and PDI range (0.2-0.5). The most suitable PA loading approach was based on the expectation that increasing PA concentration would enhance the negative surface charge (zeta potential). However, once the PA loading reached the saturation, no further increase in negativity was observed. Notably, the EE% of PA-loaded niosomes was not calculated, as continuous negativity in the zeta potential was used as an indicator of loading capacity. Although all formulations exhibited an increasing trend in negative charge upon PA loading, 0.5 % PA formulation consistently maintained a stable negative zeta potential across all niosome types, without inducing significant changes in vesicle size or increasing polydispersity. Therefore, this formulation was selected for subsequent Ab and Fab conjugation experiments.

For the mAb/Fab coupling reaction, the total PA-loaded niosome concentration was maintained as specified in Table 1. However, the mAb/Fab concentration required optimization, as it significantly

influenced the physicochemical properties. To achieve the desired physicochemical characteristics while ensuring consistency with Nio^{UV}- $^{
m NBS}$, three different mAb and Fab concentrations (0.05 mg/mL, 0.1 mg/ mL, and 0.2 mg/mL) were tested, maintaining the same FITC concentration inside the niosomes to avoid differences in cellular responses between Nio^{UV-NBS} and Nio^{EDC/NHS} formulations. The impact of mAb and Fab concentrations on the physicochemical properties of PA-loaded niosomes was assessed (Fig. S9). The results demonstrated a proportional increase in particle size with increasing mAb and Fab concentrations. The size distribution profile (Fig. S9b) indicated that the optimal mAb and Fab concentration for all Nio EDC/NHS formulations was $0.05\ mg/mL$. However, Nio-3 and Nio-4 could accommodate $0.1\ mg/mL$ while maintaining the desired physicochemical properties. Fig. S9c shows that all formulations remained within the 0.2-0.5 PDI range across different mAb and Fab loads. The zeta potential was expected to be neutral upon successful conjugation of mAbs and Fabs to PA-loaded niosomes (Fig. S9d). Considering both size and zeta potential, only the Nio-1-Fab conjugation could accommodate a higher antibody load, but 0.05 mg/mL yielded the most optimized results for subsequent Nio EDC/ NHS formulations. It is important to note that in EDC/NHS IN formulations, further optimization of antibody and antibody fragment concentrations was required after incorporating FITC at a fixed concentration (0.05 % FITC, as determined in our previous study (Cakir et al., 2024)) into 0.5 % PA-loaded niosomes, where the desired physicochemical properties could not initially be achieved.

Optimized Nio^{UV-NBS} and Nio^{EDC/NHS} formulations were synthesized and characterized using DLS, as shown in Fig. 3. The results indicate that, particularly for Nio-1 and Nio-2, conjugation with mAb and/or Fab using either the UV-NBS or EDC/NHS strategy resulted in the desired size (100–200 nm), PDI range (0.2–0.5), and near-neutral surface charge. Further cellular binding and uptake assessments were conducted for all formulations to determine the most effective conjugation strategy and identify the IN formulations with the highest potential for therapeutic applications.

3.1.3. Cellular uptake and binding of mAb/Fab-loaded INs

To assess the cellular responses of IN formulations generated through EDC/NHS and UV-NBS conjugation methods, two detection strategies were employed: (i) detection of antibodies on the niosomal formulations using a fluorescently tagged secondary antibody, and (ii) FITC loading of the INs. The optimization protocols and characterization data for the FITC-loaded INs are provided in Figs. S10 and S11. The encapsulation efficiency (EE%) of FITC in the IN formulations (Nio-1, Nio-2, Nio-3, and Nio-4) was determined for each niosome formulation after conjugation with mAb or Fab using either UV-NBS or EDC/NHS chemistry. The EE% was greater than 50 % for all formulations, with Nio-4-Fab and Nio-1-Fab conjugates demonstrating the highest efficiency (Fig. S11c). Supplementary Table 7 presents the EE% data for FITC encapsulation in each formulation. Using the standard curves from Fig. S11, Supplementary Table 8 was generated to list the mAb and Fab CE% and EE% values for each IN formulation produced by the EDC/NHS and UV-NBS methods. The UV-NBS method for incorporating mAb and Fabs into the niosomes resulted in significantly higher encapsulation efficiency, ranging from 58 % to 98 %, whereas EDC/NHS yielded encapsulation efficiencies between 1 % and 11 %.

Determining the cellular binding and uptake profiles of INs is essential for evaluating their therapeutic potential and specificity. Since Bevacizumab has been approved for treating recurrent GBM (Arevalo et al., 2019; Gil-Gil et al., 2013). U87 cells were used to assess the binding and uptake profiles of Bevacizumab mAb or its Fab fragment conjugated INs (Fig. 4). A similar analysis was also performed on healthy endothelial cells (HUVEC), and the results are provided in Fig. S13.

In all experiments, only mAb and Fab (without noisome formulations) cellular binding signals served not only as a comparison to control groups but also as reference profiles for the IN formulations. Based on the overall results from U87 cells (Fig. 4), Fab fragments showed less binding signal than the complete antibody in the original therapeutic (without conjugating into niosomes). Except for Nio-4 Fab conjugation, the remaining IN formulations for each conjugation exhibited trends similar to the original Fab in the UV-NBS method. Notably, Nio-3 Fab displayed a lower binding signal than the original Fab in glioma cells.

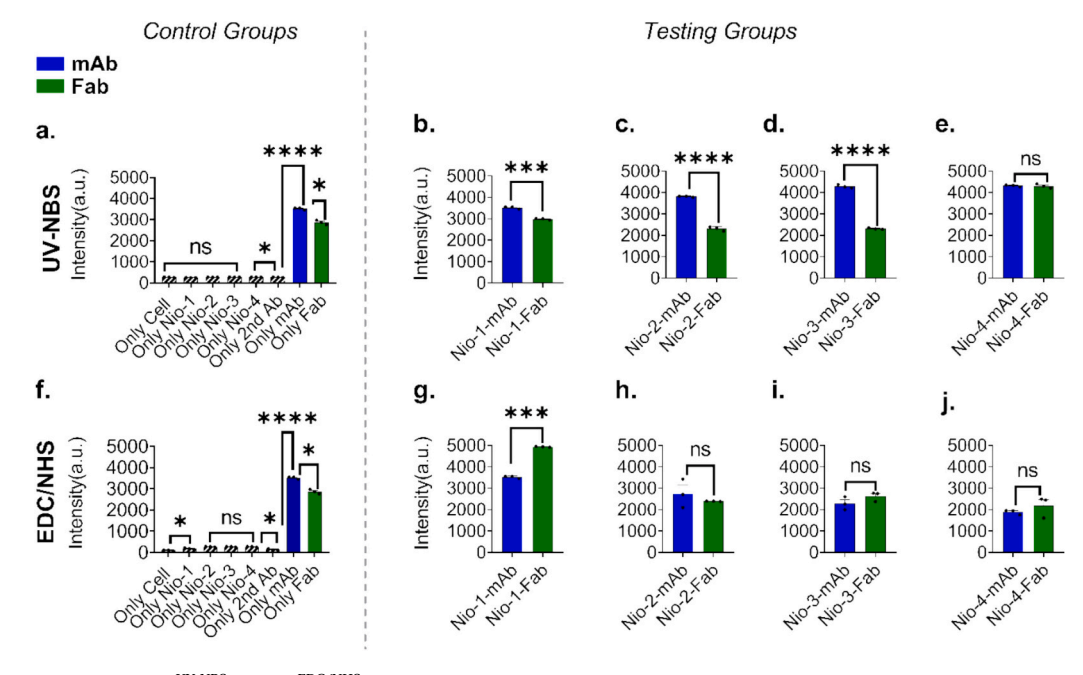


Fig. 4. Cellular binding profile of Nio^{UV-NBS} and Nio^{EDC/NHS} in U87 cell lines. a. Control groups without antibody and with antibody without nanocarrier conjugation in UV-NBS conjugation. b. UV-NBS conjugation of Nio-1 mAb and Fab, c. UV-NBS conjugation of Nio-2 mAb and Fab. d. UV-NBS conjugation of Nio-3 mAb and Fab. e. UV-NBS conjugation of Nio-4 mAb and Fab. f. Control groups without antibody and with antibody without nanocarrier conjugation in EDC/NHS conjugation. g. EDC/NHS conjugation of Nio-1 mAb and Fab, h. UV-NBS conjugation of Nio-2 mAb and Fab. i. EDC/NHS conjugation of Nio-3 mAb and Fab, j. EDC/NHS conjugation of Nio-4 mAb and Fab.

Conversely, in the EDC/NHS method, Nio-1 Fab demonstrated superior cancer cell binding compared to the other IN formulations. To predict the actual effect of the IN formulations in both UV-NBS and EDC/NHS conjugation strategies, it was necessary to determine the number of antibodies per niosome. The number of antibodies per niosome for each formulation was calculated for both UV-NBS and EDC/NHS strategies and is provided in Supplementary Tables 9 and 10, respectively. For UV-NBS, the number of antibodies was recorded as 7.93, which was lower than in the other IN formulations with Fab conjugates, yet it exhibited a higher binding signal. This finding partially supports the success of the Nio-4 Fab conjugate prior to toxicity analysis. For the EDC/NHS results, the number of antibodies per niosome was recorded as 2.16 for Fab conjugates, confirming that Nio-1 Fab exhibited higher binding signals compared to the other IN formulations, despite having fewer antibodies per niosome. While overexpressed VEGF signaling on cancer cell surfaces is known to result in higher binding signals than on healthy endothelial cells, Fab fragments are more diffuse than the complete mAb, which may contribute to reduced cell death due to the lower observed binding signal.

Considering the downstream signaling of mature VEGF found in its soluble form, it is important to note that immature VEGF signaling also exists within the intracellular environment. Therefore, determining the intracellular behavior of Bevacizumab and its IN formulations through cellular uptake assays is significant. Before delving into the interpretation of the cellular uptake results, it is necessary to first discuss VEGF signaling in glioma and endothelial cells. In glioma cells, two main VEGF signaling pathways are involved: autocrine signaling and glioma-induced angiogenesis. In autocrine signaling, glioma cells overexpress

VEGF due to the hypoxic conditions within the tumor microenvironment. This overexpression is driven by transcription factors such as HIF-1α (hypoxia-inducible factor 1-alpha), which upregulate VEGF production. VEGF can then bind to VEGFR-2 (vascular endothelial growth factor receptor 2) or other VEGFRs on the glioma cells themselves, forming an autocrine loop. This signaling promotes glioma cell proliferation, survival, invasion, and resistance to apoptosis. Therefore, the expected profile of complete uptake in U87 cells can only be confirmed through cellular toxicity assays. However, the cellular uptake results in endothelial cells contribute to the existing literature on VEGF signaling. Previous studies have found that cellular uptake in U87 cells, which predominantly contain mature and soluble VEGF in the extracellular environment, results in less intracellular VEGF signal compared to endothelial cells, as shown in Fig. S14. On the other hand, while Bevacizumab targets tumor-induced angiogenesis, systemic VEGF inhibition may affect normal physiological angiogenesis, particularly in processes like wound healing or tissue repair. Thus, the expected uptake results in endothelial cells indicated Bevacizumab's prevention of VEGF binding to VEGFR-2, effectively shutting down angiogenesis. This inhibition limits the formation of new blood vessels, depriving the tumor of oxygen and nutrients. However, the lack of a drastic difference in signal between glioma and endothelial cells, as shown in Fig. S14, suggests that further investigation into the cellular toxicity profile is needed to draw more definitive conclusions.

3.1.4. Cytotoxicity of NioUV-NBS and NioEDC/NHS formulations

To better understand the superior IN formulations, cellular binding and uptake results were complemented with cellular cytotoxicity assays,

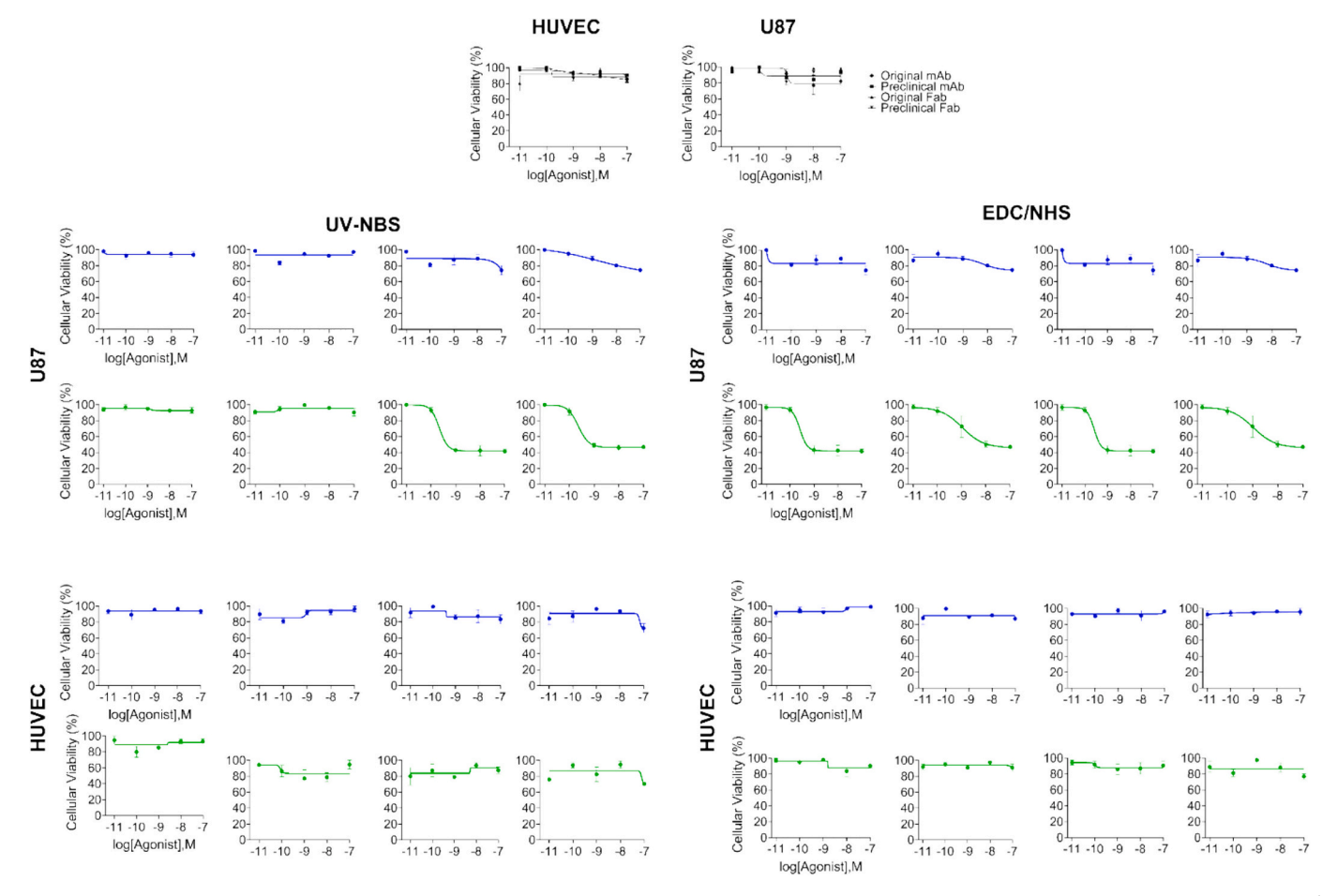


Fig. 5. Cellular toxicity assay performed for UV-NBS and EDC/NHS mAb/Fab INs in HUVEC and U87 cell lines. 24-h incubated 96-well plates are used and 1.0×10^4 cells/well are seeded equally to each well. At the top, original mAb, original Fab, preclinical mAb and preclinical Fab products are demonstrated. UV-NBS conjugated INs are indicated in the left corner while EDC/NHS conjugated INs are given in the right corner.

as demonstrated in Fig. 5. At the top of Fig. 5, control groups represent the toxicity profiles of the original and biosimilar mAb and Fab, while the remaining data show IN toxicity profiles. The results are presented on the left for UV-NBS and on the right for EDC/NHS conjugates, for both cancer and healthy cell lines.

Bevacizumab is primarily used to inhibit angiogenesis in tumors and does not exert direct cytotoxic effects on cancer cells. Although some studies have investigated its potential toxicity in U87 cells, its primary mechanism of action involves neutralizing VEGF, thereby preventing new blood vessel formation rather than directly inducing cell death (Mesti et al., 2014). Our findings confirm that Bevacizumab did not exhibit cytotoxicity in U87 cells. The absence of direct cytotoxicity in U87 cells may be due to Bevacizumab's mechanism of action, which inhibits angiogenesis without directly targeting glioma cells or disrupting the VEGF autocrine loop.

Additionally, U87 cells employ resistance mechanisms, including alternative pro-angiogenic pathways, high VEGFR expression, intracellular VEGF pools, and hypoxia-induced VEGF overexpression. Their metabolic shift to glycolysis (Warburg effect) further reduces dependence on VEGF signaling. Additionally, experimental factors such as exposure time, Bevacizumab concentration, and culture conditions may also contribute to the observed effects. To address potential limitations related to experimental conditions, Table 2 provides a comparison of the Bevacizumab concentrations used in this study with previously reported ranges.

As shown in Table 2, the concentrations of Bevacizumab used in various studies differ; however, the outcomes align with our findings comparing the toxicity profiles of the original and biosimilar formulations. Notably, certain IN formulations generated via UV-NBS conjugation exhibited enhanced toxicity compared to their unconjugated counterparts. Compared to mAb-conjugated INs, Fab-containing IN formulations demonstrated selective toxicity, exhibiting no adverse effects on healthy endothelial cells while inducing cytotoxicity in U87 cells at higher concentrations.

The UV-NBS conjugation method, which enables site-specific binding of Bevacizumab to niosomal nanocarriers, showed greater promise than randomized conjugation approaches. While all Fab-IN formulations generated through EDC/NHS chemistry exhibited toxicity toward U87 cells, repeated toxicity assays conducted on different days revealed significant variability and higher viability errors across wells. However, the Nio-1 Fab formulation conjugated via EDC/NHS demonstrated

Table 2Experimental conditions and outcome records of Bevacizumab related to glioma cells.

Cell Line	Cell Type	Bevacizumab Dosage	Outcomes	
U87 and U251	Glioblastoma	5–25 μg/mL	No significant cytotoxicity in 2D culture; anti angiogenic effects observed in 3D spheroid cocultures (Simon et al., 2014) Cytotoxicity observed in 3D spheroids demonstrated reduced VEGF-driven angiogenesis but not effect in 2D monolayers (Tamura et al., 2017)	
U87 and T98G	Glioblastoma	1–50 μg/mL		
U87 and GSCs	Glioblastoma stem cells	500–1000 μg/ mL	Bevacizumab induced moderate reduction in GSC proliferation, but the effect was VEGF dependent (Smolenschi et al., 2023)	
U87	Glioblastoma	25–100 μg/mL	Anti-angiogenic activity observed, but no cytotoxic effect on U87 directly (Diaz et al., 2017)	
U87 and C6	Rat glioma	25–200 μg/mL	Reduction of angiogenesis but no effect on glioma proliferation (De Groot et al., 2010)	

consistent toxicity profiles across all replicates, making it a promising candidate for potential glioblastoma therapy. Among the site-specific IN formulations, both Nio-4 mAb and Nio-4 Fab exhibited selective cytotoxicity toward U87 cells while sparing healthy endothelial cells.

Notably, the cytotoxic effects observed with antibody- and Fab-conjugated niosomes (INs) should be interpreted in the context of nanoparticle-based avidity. While the free forms of Bevacizumab and its Fab fragment are generally well tolerated (Table 2), their conjugation to nanoparticles enables multivalent presentation of targeting ligands, enhancing binding strength and cellular interaction through the avidity effect. This multivalency can lead to increased receptor clustering and internalization, potentially triggering more pronounced biological responses—even at lower apparent concentrations compared to free antibodies. Therefore, the observed cytotoxicity is likely a combined outcome of nanoparticle composition, surface characteristics, and enhanced cellular engagement due to avidity. This distinction is critical when evaluating the therapeutic index and safety profile of targeted nanoconjugates.

While these optimized IN formulations present promising insights for glioblastoma treatment, further downstream analyses and non-clinical evaluations are recommended to support their development as viable therapeutic candidates. While long-term stability studies are essential for clinical translation, this study focused on evaluating antibody-conjugation strategies on niosomal formulations within short experimental timeframes (\leq 24 h). It is worth noting that the stability of our base niosomal systems (Cakir et al., 2024) has been previously validated for up to 35 days, and further studies will be needed to determine how antibody conjugation impacts long-term physicochemical and biological stability. To further investigate the effects of Bevacizumab, the use of 3D models could provide a more physiologically relevant system that better mimics VEGF gradients and hypoxic conditions, potentially revealing additional insights into its impact on glioma cells, and those studies are ongoing in our laboratories.

4. Conclusion

This study presents novel conjugation strategies for integrating monoclonal antibodies (mAbs) and Fab fragments with niosomes, establishing a promising alternative to immunoliposomes for targeted drug delivery. Through site-specific and randomized conjugation methods, we successfully developed stable antibody-conjugated niosomes with physicochemical properties favorable for therapeutic applications. Notably, Fab-conjugated niosomes exhibited selective cytotoxicity toward U87 glioblastoma cells while sparing healthy endothelial cells, demonstrating their potential for glioblastoma treatment. The enhanced efficacy of site-specific conjugation via UV-NBS suggests its superiority over conventional methods, offering improved therapeutic outcomes. These findings provide valuable insights into antibody-based nanocarriers and highlight the need for further preclinical evaluations to optimize their application in glioblastoma therapy and beyond.

CRediT authorship contribution statement

Nilufer Cakir: Writing – review & editing, Writing – original draft, Visualization, Methodology, Investigation, Formal analysis, Data curation. Hatice Oncel: Writing – review & editing, Resources, Investigation, Data curation. Aylin Ozkan: Writing – review & editing, Resources, Investigation, Data curation. Dilan Bicak: Writing – review & editing, Resources, Investigation, Data curation. Sibel Akgun Bas: Writing – review & editing, Resources, Investigation, Data curation. Nur Mustafaoglu: Writing – review & editing, Visualization, Supervision, Resources, Funding acquisition, Conceptualization.

Funding

The authors would like to express their gratitude to the EMBO Installation Grant (Project No. IG-5352-2023, awarded to N.M.), and the ERC Starting Grant (Project No. 101116521, awarded to N.M.) for their financial support. Additionally, they acknowledge the support of the TÜBİTAK 2244 Industrial PhD Fellowship (Project No. 118C149, awarded to N.C.). N.M. also extends appreciation to the BAGEP Award of the Science Academy and the TÜBA-GEBİP Award of the Turkish Academy of Sciences for their contributions.

Declaration of competing interest

Nur Mustafaoglu reports financial support was provided by European Molecular Biology Organization. Nur Mustafaoglu reports financial support was provided by European Research Council. Nilufer Cakir reports financial support was provided by Scientific and Technological Research Council of Turkey. If there are other authors, they declare that they have no known competing financial interests or personal relationships that could have appeared to influence the work reported in this paper.

Acknowledgments

The authors sincerely thank Faculty of Engineering and Natural Sciences (FENS) at Sabancı University and ILKO Biotech Company for providing materials and granting access to their facilities.

Appendix A. Supplementary data

Supplementary data to this article can be found online at https://doi.org/10.1016/j.ijpx.2025.100367.

Data availability

Data will be made available on request.

References

- Alves, N.J., Stimple, S.D., Handlogten, M.W., Ashley, J.D., Kiziltepe, T., Bilgicer, B., 2012. Small-molecule-based affinity chromatography method for antibody purification via nucleotide binding site targeting. Anal. Chem. 84, 7721–7728. https://doi.org/10.1021/ac300952r.
- Alves, N.J., Champion, M.M., Stefanick, J.F., Handlogten, M.W., Moustakas, D.T., Shi, Y., Shaw, B.F., Navari, R.M., Kiziltepe, T., Bilgicer, B., 2013a. Selective photocrosslinking of functional ligands to antibodies viatheconserved nucleotide binding site. Biomaterials 34, 5700–5710. https://doi.org/10.1016/j.biomaterials.2013.03.082.
- Alves, N.J., Mustafaoglu, N., Bilgicer, B., 2013b. Oriented antibody immobilization by site-specific UV photocrosslinking of biotin at the conserved nucleotide binding site for enhanced antigen detection. Biosens. Bioelectron. 49, 387–393. https://doi.org/ 10.1016/j.bios.2013.05.052
- Alves, N.J., Mustafaoglu, N., Bilgicer, B., 2014. Conjugation of a reactive thiol at the nucleotide binding site for site-specific antibody functionalization. Bioconjug. Chem. 25, 1198–1202. https://doi.org/10.1021/bc500211d.
- Arevalo, O.D., Soto, C., Rabiei, P., Kamali, A., Ballester, L.Y., Esquenazi, Y., Zhu, J.-J., Riascos, R.F., 2019. Assessment of Glioblastoma Response in the Era of Bevacizumab: Longstanding and Emergent challenges in the Imaging Evaluation of Pseudoresponse. Front. Neurol. 10, 460. https://doi.org/10.3389/ fneur.2019.00460.
- Arruebo, M., Valladares, M., González-Fernández, Á., 2009. Antibody-Conjugated Nanoparticles for Biomedical applications. J. Nanomater. 2009, 439389. https://doi. org/10.1155/2009/439389.
- Bartelds, R., Nematollahi, M.H., Pols, T., Stuart, M.C.A., Pardakhty, A., Asadikaram, G., Poolman, B., 2018. Niosomes, an alternative for liposomal delivery. PloS One 13, e0194179. https://doi.org/10.1371/journal.pone.0194179.
- Bernard-Arnoux, F., Lamure, M., Ducray, F., Aulagner, G., Honnorat, J., Armoiry, X., 2016. The cost-effectiveness of tumor-treating fields therapy in patients with newly diagnosed glioblastoma. Neuro Oncol. 18, 1129–1136. https://doi.org/10.1093/ neuonc/now102.
- Bordeau, B.M., Balthasar, J.P., 2021. Strategies to enhance monoclonal antibody uptake and distribution in solid tumors. Cancer Biol. Med. 18, 649–664. https://doi.org/ 10.20892/j.issn.2095-3941.2020.0704.

- Cakir, N., Ozturk, N., Kara, A., Zarrabi, A., Mustafaoglu, N., 2024. Optimizing niosomal formulations for enhanced cellular applications. Adv Pharmacol Pharm Sci 2024. https://doi.org/10.1155/2024/9933465.
- Chiu, M.L., Goulei, D.R., Teplyakov, A., Gilliland, G.L., 2019. Antibody structure and function: the basis for engineering therapeutics. Antibodies 8. https://doi.org/ 10.3390/antib8040055.
- Cohen, M.H., Shen, Y.L., Keegan, P., Pazdur, R., 2009. FDA drug approval summary: bevacizumab (Avastin®) as treatment of recurrent glioblastoma multiforme. The oncologist 14 (11), 1131–1138. https://doi.org/10.1634/theoncologist.2009-0121
- De Groot, J.F., Fuller, G., Kumar, A.J., Piao, Y., Eterovic, K., Ji, Y., Conrad, C.A., 2010. Tumor invasion after treatment of glioblastoma with bevacizumab: Radiographic and pathologic correlation in humans and mice. Neuro Oncol. 12, 233–242. https://doi.org/10.1093/neurorc/nop027.
- De, A., Venkatesh, N., Senthil, M., Sanapalli, B.K.R., Shanmugham, R., Karri, V.V.S.R., 2018. Smart niosomes of temozolomide for enhancement of brain targeting. Nanobiomedicine (Rij) 5. https://doi.org/10.1177/1849543518805355, 1849543518805355.
- Diaz, R.J., Ali, S., Qadir, M.G., De La Fuente, M.I., Ivan, M.E., Komotar, R.J., 2017. The role of bevacizumab in the treatment of glioblastoma. J. Neurooncol. https://doi. org/10.1007/s11060-017-2477-x.
- Eloy, J.O., Petrilli, R., Trevizan, L.N.F., Chorilli, M., 2017. Immunoliposomes: a review on functionalization strategies and targets for drug delivery. Colloids Surf. B Biointerfaces 159, 454–467. https://doi.org/10.1016/j.colsurfb.2017.07.085.
- Garcia, J., Hurwitz, H.I., Sandler, A.B., Miles, D., Coleman, R.L., Deurloo, R., Chinot, O. L., 2020. Bevacizumab (Avastin®) in cancer treatment: a review of 15 years of clinical experience and future outlook. Cancer Treat. Rev. 86, 102017. https://doi.org/10.1016/j.ctrv.2020.102017.
- Gharbavi, M., Amani, J., Kheiri-Manjili, H., Danafar, H., Sharafi, A., 2018. Niosome: a Promising Nanocarrier for Natural Drug delivery through Blood-Brain Barrier. Adv. Pharmacol. Sci. 2018. https://doi.org/10.1155/2018/6847971.
- Gil-Gil, M.J., Mesia, C., Rey, M., Bruna, J., 2013. Bevacizumab for the treatment of glioblastoma. Clin Med Insights Oncol 7, 123–135. https://doi.org/10.4137/CMO. \$8503
- Ibrahim Bekraki, A., 2020. In: Kesharwani, P.B.T.N.B.A. (Ed.), Chapter 7 Liposomes-and niosomes-based drug delivery systems for tuberculosis treatment. Academic Press, pp. 107–122. https://doi.org/10.1016/B978-0-12-819811-7.00007-2.
- Kazi, K.M., Mandal, A.S., Biswas, N., Guha, A., Chatterjee, S., Behera, M., Kuotsu, K., 2010. Niosome: a future of targeted drug delivery systems. J. Adv. Pharm. Technol. Res. 1, 374–380. https://doi.org/10.4103/0110-5558.76435.
- Khoee, S., Yaghoobian, M., 2017. Chapter 6 Niosomes: a novel approach in modern drug delivery systems. In: Andronescu, E., Grumezescu, A.M.B.T.N. (Eds.), Micro and Nano Technologies. Elsevier, pp. 207–237. https://doi.org/10.1016/B978-0-323-46143-6.00006-3.
- Kirpotin, D.B., Noble, C.O., Hayes, M.E., Huang, Z., Kornaga, T., Zhou, Y., Nielsen, U.B., Marks, J.D., Drummond, D.C., 2012. Chapter seven building and characterizing antibody-targeted lipidic nanotherapeutics. In: Wittrup, K.D., Verdine, G.L. (Eds.), Methods in Enzymology. Academic Press, pp. 139–166. https://doi.org/10.1016/B978-0-12-416039-2.00007-0.
- Kontermann, R.E., 2006. Immunoliposomes for cancer therapy. Curr. Opin. Mol. Ther. 8, 39–45.
- Kumari, M., Acharya, A., Krishnamurthy, P.T., 2023. Antibody-conjugated nanoparticles for target-specific drug delivery of chemotherapeutics. Beilstein J. Nanotechnol. https://doi.org/10.3762/bjnano.14.75.
- Liga, S., Paul, C., Moacă, E.A., Péter, F., 2024. Niosomes: Composition, Formulation Techniques, and recent Progress as delivery Systems in Cancer Therapy. Pharmaceutics. https://doi.org/10.3390/pharmaceutics16020223.
- Lim, Z.F., Ma, P.C., 2019. Emerging insights of tumor heterogeneity and drug resistance mechanisms in lung cancer targeted therapy. J. Hematol. Oncol. 12, 1–18. https:// doi.org/10.1186/s13045-019-0818-2.
- Liu, F.R., Jin, H., Wang, Y., Chen, C., Li, M., Mao, S.J., Wang, Q., Li, H., 2017. Anti-cd123 antibody-modified niosomes for targeted delivery of daunorubicin against acute myeloid leukemia. Drug Deliv. https://doi.org/10.1080/10717544.2017.1333170.
- Merino, M., Zalba, S., Garrido, M.J., 2018. Immunoliposomes in clinical oncology: State of the art and future perspectives. J. Control. Release 275, 162–176. https://doi.org/ 10.1016/j.jconrel.2018.02.015.
- Mesti, T., Savarin, P., Triba, M.N., Le Moyec, L., Ocvirk, J., Banissi, C., Carpentier, A.F., 2014. Metabolic impact of anti-angiogenic agents on U87 glioma cells. PloS One 9, e99198. https://doi.org/10.1371/journal.pone.0099198.
- Mustafaoglu, N., Alves, N.J., Bilgicer, B., 2015a. Oriented Immobilization of Fab Fragments by Site-specific Biotinylation at the Conserved Nucleotide Binding Site for Enhanced Antigen Detection. Langmuir 31, 9728–9736. https://doi.org/10.1021/ acs.langmuir.5b01734.
- Mustafaoglu, N., Alves, N.J., Bilgicer, B., 2015b. Site-specific fab fragment biotinylation at the conserved nucleotide binding site for enhanced ebola detection. Biotechnol. Bioeng. 112, 1327–1334. https://doi.org/10.1002/bit.25558.
- Mustafaoglu, N., Kiziltepe, T., Bilgicer, B., 2017. Site-specific conjugation of an antibody on a gold nanoparticle surface for one-step diagnosis of prostate specific antigen with dynamic light scattering. Nanoscale 9, 8684–8694. https://doi.org/10.1039/ c7nr03096e.
- Narsinh, K.H., Perez, E., Haddad, A.F., Young, J.S., Savastano, L., Villanueva-Meyer, J.E., Winkler, E., de Groot, J., 2024. Strategies to improve drug delivery across the blood-brain barrier for glioblastoma. Curr. Neurol. Neurosci. Rep. https://doi.org/ 10.1007/s11910-024-01338-x.
- Rabenhold, M., Steiniger, F., Fahr, A., Kontermann, R.E., Rüger, R., 2015. Bispecific single-chain diabody-immunoliposomes targeting endoglin (CD105) and fibroblast

- activation protein (FAP) simultaneously. J. Control. Release 201, 56–67. https://doi.org/10.1016/j.jconrel.2015.01.022.
- Reinmuth-Selzle, K., Tchipilov, T., Backes, A.T., Tscheuschner, G., Tang, K., Ziegler, K., Lucas, K., Pöschl, U., Fröhlich-Nowoisky, J., Weller, M.G., 2022. Determination of the protein content of complex samples by aromatic amino acid analysis, liquid chromatography-UV absorbance, and colorimetry. Anal. Bioanal. Chem. 414, 4457–4470. https://doi.org/10.1007/s00216-022-03910-1.
- Reverberi, R., Reverberi, L., 2007. Factors affecting the antigen-antibody reaction. Blood Transfus. 5, 227–240. https://doi.org/10.2450/2007.0047-07.
- Rodallec, A., Brunel, J.-M., Giacometti, S., Maccario, H., Correard, F., Mas, E., Orneto, C., Savina, A., Bouquet, F., Lacarelle, B., Ciccolini, J., Fanciullino, R., 2018. Docetaxeltrastuzumab stealth immunoliposome: development and in vitro proof of concept studies in breast cancer. Int. J. Nanomed. 13, 3451–3465. https://doi.org/10.2147/ LJN.S162454.
- Rong, L., Li, N., Zhang, Z., 2022. Emerging therapies for glioblastoma: current state and future directions. J. Exp. Clin. Cancer Res. 41, 142. https://doi.org/10.1186/ s13046-022-02349-7.
- Saharkhiz, S., Nasri, N., Naderi, N., Dini, G., Ghalehshahi, S.S., Firoozbakht, F., 2024. Evaluating a targeted Palbociclib-Trastuzumab loaded smart niosome platform for treating HER2 positive breast cancer cells. Int J Pharm X 7, 100237. https://doi.org/ 10.1016/J.IJPX.2024.100237.
- Schmidt, B., Lee, H.-J., Ryeom, S., Yoon, S.S., 2012. Combining bevacizumab with radiation or chemoradiation for solid tumors: a review of the scientific rationale, and clinical trials. Curr Angiogenes 1, 169–179. https://doi.org/10.2174/
- Selis, F., Focà, G., Sandomenico, A., Marra, C., Di Mauro, C., Jotti, G.S., Scaramuzza, S., Politano, A., Sanna, R., Ruvo, M., Tonon, G., 2016. Pegylated trastuzumab fragments

- acquire an increased in vivo stability but show a largely reduced affinity for the target antigen. Int. J. Mol. Sci. 17, 1–15. https://doi.org/10.3390/ijms17040491.
- Simon, T., Coquerel, B., Petit, A., Kassim, Y., Demange, E., Le Cerf, D., Perrot, V., Vannier, J.P., 2014. Direct effect of Bevacizumab on Glioblastoma Cell Lines in Vitro. Neuromolecular Med. 16, 752–771. https://doi.org/10.1007/s12017-014-8324-8
- Smolenschi, C., Rassy, E., Pallud, J., Dezamis, E., Copaciu, R., Parker, F., Garcia, G., Lezghed, N., Colomba, E., Khettab, M., Ammari, S., Fekhi, M., Martanovschi, L., Benadhou, L., Knafo, S., Guyon, D., Cheaib, B., Dhermain, F., Dumont, S.N., 2023. Bevacizumab in real-life patients with recurrent glioblastoma: benefit or futility? J. Neurol. 270, 2702–2714. https://doi.org/10.1007/s00415-023-11600-w.
- Tamura, R., Tanaka, T., Miyake, K., Yoshida, K., Sasaki, H., 2017. Bevacizumab for malignant gliomas: current indications, mechanisms of action and resistance, and markers of response. Brain Tumor Pathol. 34, 62–77. https://doi.org/10.1007/ s10014-017-0284-x
- Wang, D., Sun, Y., Liu, Y., Meng, F., Lee, R.J., 2018. Clinical translation of immunoliposomes for cancer therapy: recent perspectives. Expert Opin. Drug Deliv. 15, 893–903. https://doi.org/10.1080/17425247.2018.1517747.
- Weathers, S.-P., Han, X., Liu, D.D., Conrad, C.A., Gilbert, M.R., Loghin, M.E., O'Brien, B. J., Penas-Prado, M., Puduvalli, V.K., Tremont-Lukats, I., Colen, R.R., Yung, W.K.A., de Groot, J.F., 2016. A randomized phase II trial of standard dose bevacizumab versus low dose bevacizumab plus lomustine (CCNU) in adults with recurrent glioblastoma. J. Neurooncol 129, 487–494. https://doi.org/10.1007/s11060-016-2195-9.
- Wiwatchaitawee, K., Quarterman, J.C., Geary, S.M., Salem, A.K., 2021. Enhancement of therapies for glioblastoma (GBM) using nanoparticle-based delivery systems. AAPS PharmSciTech 22, 71. https://doi.org/10.1208/s12249-021-01928-9.